Design and characterization of porphyrin-based photosensitizing metalloproteins integrated with artificial metalloenzymes for photocatalytic hydrogen production

Opdam, L.V.; Götzfried, S.K.; Polanco Rivas, E.A.; Bonnet, S.A.; Pandit, A.

Journal of Inorganic Biochemistry 267 (2025) 112855

Contents lists available at ScienceDirect

Journal of Inorganic Biochemistry

journal homepage: www.elsevier.com/locate/jinorgbio

Design and characterization of porphyrin-based photosensitizing metalloproteins integrated with artificial metalloenzymes for photocatalytic hydrogen production

L.V. Opdam [a,b], S.K. Goetzfried [a,c], E. Polanco [a], S. Bonnet [a], A. Pandit [a,*]

[a] Leiden Institute of Chemistry, Leiden University, Einsteinweg 55, 2300 RA Leiden, the Netherlands
[b] Bioénergétique et Ingénierie des Protéines, 13402 Marseille, France
[c] Stratingh Institute for Chemistry, University of Groningen, 9747 AG Groningen, The Netherlands

ARTICLE INFO

Keywords:
Photosensitizer
Haemoprotein
Artificial photosynthesis
Haem acquisition system Ap
Protoporphyrin IX
Earth-abundant metal

ABSTRACT

Hydrogen is regarded as a promising alternative to fossil fuels. A desirable method of its generation is via photocatalysis, combining photosensitizers and hydrogen-evolution catalysts in the presence of an electron donor. Inspired by natural photosynthesis, we designed photosensitizing artificial metalloproteins (ArMs) and integrated them with ArM-based catalysts for photocatalytic hydrogen production from water. Metal porphyrins based on protoporphyrin IX (PPIX) were employed as they are naturally abundant and are effective both as photosensitizers and hydrogen-evolution catalysts. Photosensitizing proteins were created by binding zinc (Zn) PPIX or ruthenium (Ru)PPIX to the haem acquisition system A *from Pseudomonas aeruginosa* (HasAp). The photosensitizer ArMs were combined with cobalt (Co)PPIX-myoglobin (Mb) or free CoPPIX as hydrogen evolution catalysts. We found that free CoPPIX could replace ZnPPIX or RuPPIX in HasAp, forming CoPPIX-HasAp or RuPPIX-CoPPIX-HasAp complexes with enhanced stability compared to CoPPIX-Mb. Photocatalytic hydrogen production was achieved upon irradiation at 435 nm (ZnPPIX) or 385 nm (RuPPIX), using methyl viologen as an electron carrier and triethanolamine as an electron donor. The ZnPPIX-HasAp/CoPPIX-HasAp system remained intact and active for approximately 42 h, while Ru-based systems that were excited by UV light, exhibited signs of protein cleavage upon prolonged irradiation. These results demonstrate the potential of integrating porphyrin-based ArMs for photosensitization and hydrogen evolution, with HasAp providing a robust scaffold for sustained photocatalytic activity.

1. Introduction

Finding green alternatives for the use of fossil fuels is becoming increasingly pressing [1]. Using hydrogen as an alternative to fossil fuels has been proposed in the 1970s already for the potential of this molecule as an energy carrier that produces no harmful waste products upon burning in presence of O_2 [2–4]. A desirable means of generating hydrogen is via photocatalysis [5]. This method requires a hydrogen evolution catalyst (HEC), a photosensitizer (PS), a source of electrons, and, in some cases, an electron relay [6]. Homogeneous photocatalysis is an attractive means of testing the catalytic activity and stability of new HECs that can later on be included in devices [7]. Metal porphyrins, especially those hosting a redox-active metal centre, can serve as HEC in a photocatalytic mixture [8–15]. For their solubility in aqueous solutions, protein-based catalysts have been designed in which the molecular catalysts are interfaced with a protein scaffold, forming artificial metalloproteins (ArMs). Successful examples of protein-based HECs incorporating cobalt catalysts for proton reduction include cobalt protoporphyrin IX (CoPPIX) in myoglobin (Mb) and myoglobin mutants [12], cobaloximes in haem oxygenase [16], CoPPIX immobilized on a

Abbreviations: ArM, Artificial metalloprotein; BCA, Bicinochonic acid; CD, Circular dichroism; DLS, Dynamic light scattering; HasAp, Haem acquisition system A from *Pseudomonas Aeruginosa*; HEC, Hydrogen evolution catalyst; ICP-MS, Inductively coupled plasma mass spectrometry; LED, Light emitting diode; Mb, Myoglobin; MV^{2+}, Methyl viologen; NanoDSF, Nano differential scanning fluorimetry; PPIX, Protoporphyrin IX; PS, Photosensitizer; QY, Quantum yield; SD, Sacrificial donor; SEC-MALS, Size exclusion chromatography multiangle light scattering; SN-PAGE, Semi-native polyacrylamide gel electrophoresis; TEOA, Triethanolamine; Ti, Inflection temperature; TOF, Turnover frequency; TON, Turnover number; TRSPC, Time-Resolved Single Photon Counting..

* Corresponding author.
E-mail address: a.pandit@lic.leidenuniv.nl (A. Pandit).

https://doi.org/10.1016/j.jinorgbio.2025.112855
Received 29 September 2024; Received in revised form 28 January 2025; Accepted 11 February 2025
Available online 15 February 2025

recombinant silk protein film [14] and cobalt porphyrins attached to small synthetic peptides that reached very high turnover numbers for hydrogen evolution catalysis [17,18]. The role of the PS is often filled by either ruthenium trisbipyridine, $Ru(bpy)_3^{2+}$ [19]. Typically, this photosensitizer has to be added in about 1000-fold excess to the catalyst solutions for optimal catalytic performances, and its photo decomposition is a limiting factor for sustained photocatalytic activity [23]. An alternative photosensitizer is the soluble zinc porphyrin derivative tetrakis (1-methylpyridinium-4-yl) porphinato zinc(II) ($ZnTMPyP^{4+}$) [20,21]. While ruthenium appears as a non-sustainable solution due to the low concentration of this metal in the earth crust, the latter is based on a more abundant first-row transition metal, which is more promising for real-world energy applications [21,22]. To drive a photocatalytic hydrogen evolution reaction in homogeneous conditions a PS should have a long excited-state lifetime, a strong absorbance in the UV-VIS range, good (photo)stability, and solubility in aqueous solutions [8]. Metal porphyrins form suitable PS based on their long triplet lifetimes, strong absorbance in the visible range, and good photostability, but they are often poorly soluble in aqueous solution, which typically leads to aggregation and loss of their sensitizing properties [8]. To resolve that problem, soluble porphyrin derivatives have been prepared [8,21,24], but often at high synthetic cost [8]. It is therefore advantageous to use protoporphyrin IX (PPIX), the most abundant porphyrin in nature, directly in photocatalysis without modification of its organic backbone [25].

Inspired by nature, we here aimed to create an ArM-based system for photocatalytic hydrogen evolution from water through inter-protein electron transfer via an electron carrier. In natural photosynthesis, photocatalytic reactions are driven by photosensitizing and catalytic cofactors bound to different protein units that are connected via intra- or inter-protein electron transfer. In artificial photosynthesis, this concept has been less explored. In biohybrid approaches, Photosystem I or the electron shuttle protein flavodoxin were used to successfully create complexes that combined photosensitizing and hydrogen evolution catalysis via intra-protein [26,27] or inter-protein electron transfer [28]. Our strategy was to control the solubility and activity of porphyrin-based PS by incorporating them into a protein scaffold [29], and to combine those with an established hydrogen evolution catalyst, creating ArM-based systems for photocatalytic hydrogen production. We used the ability of PPIX metal complexes to bind to a large range of haem-binding *apo*-proteins, which allowed us to form photoactive, water-soluble adducts [22,26]. To keep the attractive properties of the PS, though, not every metal can be bound to PPIX. Essentially, diamagnetic metal ions such as Zn^{2+} or Ru^{2+} are ideal, as they do not modify the lifetime of the porphyrin excited state too much [30]. For example, porphyrin-based protein-PS containing ZnPPIX have been prepared for photosensitizing hydrogen evolution by platinum nanoparticles [31,32]. The protein scaffold had to be robust, capable of binding metal porphyrin complexes, and provide opportunities for further optimization e.g. by site-directed mutagenesis. Therefore, we selected the haem acquisition system Ap from *pseudomonas aeruginosa* (HasAp, Fig. 1A and B). This protein is a transient haem-binding protein with an opening and closing mechanism to capture haem in its binding pocket [33]. HasAp has evolved for stealing haem from host organisms, therefore it has a strong affinity for binding haem [34–36] as well as a high thermal stability, as it does not denature below 90 °C in the haem bound state [37]. HasAp has also been demonstrated to be capable of binding metal compounds different from haem [38–40]. Two HasAp-based PS were hence designed: **ZnPPIX-HasAp**, coordinating ZnPPIX (Fig. 1D), a compound commonly used as a PS [31,32]; and **RuPPIX-HasAp**, coordinating RuPPIX (Fig. 1E). Ruthenium porphyrin has been investigated for use in photodynamic therapy [41]. Further, ruthenium mesoporphyrin bound to myoglobin (Mb), noted RuPPIX-Mb, has been used for sensing dioxygen in biological media [42]. These reports suggest a long lifetime advantageous for redox photocatalysis. In the next step, the PS ArMs were mixed with PPIX-based HEC ArMs in the presence of an electron mediator to create a fully protein-based system for photocatalytic hydrogen evolution from water. Hereto the **ZnPPIX-HasAp** and **RuPPIX-HasAp** PS were combined with CoPPIX in solution or with CoPPIX bound to myoglobin (**CoPPIX-Mb**, Fig. 1C and F) [43]. Photocatalytic hydrogen activity has been previously demonstrated using this HEC [12]. Hydrogen evolution was measured in the presence of

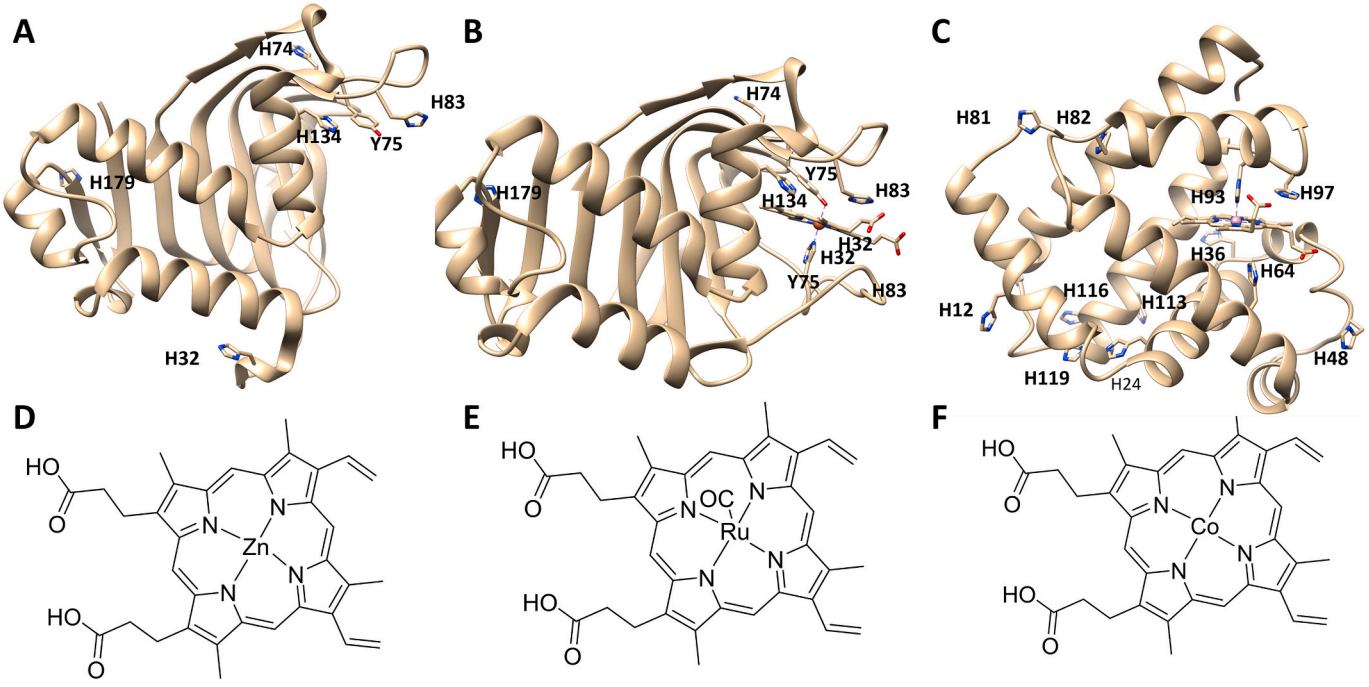

Fig. 1. **A** apoHasAp (PDB-ID 3MOK [38]), **B** holoHasAp (PDB_ID 3ELL [46]) and **C** **CoPPIX-Mb** (PDB-ID 1YOG [47]) with the binding pocket tyrosine of HasAp and all histidines shown in sticks and labelled explicitly. D—F show the structures of zinc protoporphyrin IX (**D**), ruthenium protoporphyrin IX (**E**) and cobalt protoporphyrin IX (**F**).

triethanolamine (TEOA) as sacrificial donor and methyl viologen in the form of MV^{2+} to shuttle electrons between the HEC and PS ArMs. Methyl viologens is a classical bi-cationic molecular electron relay that can be photo reduced into its cation radical $MV^{\bullet+}$ [44,45]. We demonstrate that our combined PS/HEC ArM systems are capable of light-driven hydrogen generation in the presence of MV and TEOA. A stability analysis of the ArMs before, during, and after photocatalysis was performed to evaluate their suitability for sustained photocatalysis.

2. Results

2.1. Design and characterization of the ArMs

2.1.1. Protein binding, thermostability and stoichiometry of the porphyrin ligands

Incorporation of RuPPIX and ZnPPIX in HasAp was achieved by the following approach. The haem-free (*apo*) form of HasAp was prepared as described in Opdam et al 2022 [39]. To determine the optimal conditions for the reaction with ZnPPIX and RuPPIX, the metal porphyrins were mixed with *apo*HasAp in different protein:porphyrin ratios. Optimization of ligand binding reactions are described in the Materials and Methods section in the SI (see also Fig. S2 and S3). CoPPIX bound to *apo*Mb was prepared according to methods from literature (Sommer et al. 2014) [12], using a 1:10 ratio and reacting Mb and CoPPIX at room temperature for 1 h. A binding ratio of Mb:CoPPIX of 1:3.2 for **CoPPIX-Mb** was determined using the reported extinction coefficient of CoPPIX of $\varepsilon_{426} = 170{,}000\ M^{-1}\ cm^{-1}$ [12] and using a Bicinochonic acid (BCA, Bio-Rad, California, USA) kit for determining the protein concentration (see Table S1). The binding stoichiometries of **ZnPPIX-HasAp** and **RuPPIX-HasAp**, produced under optimal binding conditions, were determined using a BCA kit in combination with inductively coupled plasma mass spectrometry (ICP-MS), since there are no reported extinction coefficients available for these ArMs. HasAp was found to bind to ZnPPIX in a 1:1.1 ratio and to RuPPIX in a 1:2.4 ratio (Table S1). We conclude that **ZnPPIX-HasAp** contained ~1 ZnPPIX, **RuPPIX-HasAp** contained ~2 RuPPIX and **CoPPIX-Mb** contained ~3 CoPPIX *per* protein.

The stability of the ArMs was tested using nano differential scanning fluorimetry (NanoDSF) (Fig. S4 and S5). In this technique, a change in the inflection temperature (T_i) for protein unfolding indicates a change in protein stability. *Apo*HasAp and *apo*Mb had a T_i of 70 °C. Increased thermostability up to 85 °C was observed for *apo*HasAp reacted with RuPPIX (Fig. S4A, incubation at 37 °C and B, incubation at 50 °C), or reacted with ZnPPIX (Fig. S4C, incubation at 4 °C and D incubation at 37 °C). The thermostability for *apoMb* reacted with CoPPIX reached 82 °C (Fig. S4E). The thermostabilities of the ArMs are presented in Table 1.

Circular dichroism (CD) spectra of the produced ArMs confirmed that binding of the artificial porphyrin ligands did not lead to protein unfolding (Fig. S6) as characteristic negative signals at ~211 and ~ 222 nm, representative of α-helical structure [46], were maintained. *Apo* and *holo*HasAp have different folds, related to the open and closed state of the protein [38,48], explaining the differences in their CD spectra (Fig. S6 A,B, red and black curves). *Apo* HasAp contains a negative band at ~219 nm, which could represent the contribution of *β*-sheet conformation, while *holo*HasAp has more pronounced α-helical character. Binding of the RuPPIX or ZnPPIX to *apo* HasAp resulted in CD spectra with increased α-helical character, though to a different extend. The CD spectra of **RuPPIX-HasAp** and **ZnPPIX-HasAp** contained both features of *apo* and *holo* HasAp and reflect some structural perturbation caused by the incorporation non-native cofactors (blue curves in Fig. S6A, **RuPPIX-HasAp** and S6B, **ZnPPIX-HasAp**). The CD spectra of *apo* and *holo*Mb (black and red curves in Fig. S6C) were typical of α-helical protein and a similar spectrum was produced for **CoPPIX-Mb** (Fig. S6C, blue curve).

Table 1
Thermostability of the ArMs. Inflection temperatures were determined by nanoDSF using a Hill Equation fit of the raw data in Fig. S5.

Sample	T_i [°C]
Apo HasAp	70
Holo HasAp	No inflection point detected
ZnPPIX-HasAp	85
RuPPIX-HasAp	85
CoPPIX-Mb	82

2.1.2. Mixing of CoPPIX with ZnPPIX-HasAp and RuPPIX-HasAp results in CoPPIX binding to HasAp

During photocatalytic experiments, the HasAp photosensitizing ArMs were mixed with either **CoPPIX-Mb** or CoPPIX. We found evidence that in these cases, CoPPIX could bind to HasAp, via partial exchange with ZnPPIX or RuPPIX as outlined below. Fig. 2 shows the result of stepwise titration of CoPPIX to **ZnPPIX-HasAp** (Fig. 2A) and to **RuPPIX-HasAp** (Fig. 2C). The absorbance maxima of **ZnPPIX-HasAp**, **RuPPIX-HasAp**, and CoPPIX are 427 nm, 400 nm, and 418 nm respectively. Fig. 2B and D present difference spectra subtracting the individual spectra of equivalent amounts of **ZnPPIX-HasAp** and CoPPIX in solution (Fig. 2B) and of **RuPPIX-HasAp** and CoPPIX in solution in (Fig. 2D), from the spectra of the titration mixtures. In the difference spectra in Fig. 2B, a decrease was observed at 427 nm and a small increase at 442 nm. The former suggested release of ZnPPIX and its precipitation from solution, while the latter could indicate that CoPPIX bound to HasAp. A distinct change in the Q-bands was also observed: the difference spectra in Fig. 2D show a decrease of signal at 400 nm, consistent with loss of RuPPIX and its precipitation from solution, as well as an increase at 431 nm that could represent CoPPIX bound to HasAp. To test how firmly CoPPIX would bind to HasAp, solutions of the **ZnPPIX-HasAp** and **RuPPIX-HasAp** ArMs mixed with CoPPIX were purified over a desalting column to remove unbound cofactors and protein to porphyrin stoichiometries were determined using a BCA kit (Bio Rad) and ICP-MS (Table S1). The resulting protein and ligand ratios of the mixtures of **RuPPIX-HasAp**/CoPPIX and **ZnPPIX-HasAp**/CoPPIX, determined by ICP-MS, were HasAp:RuPPIX:CoPPIX 1:2.0:0.5 and HasAp:ZnPPIX:CoPPIX 1:0.6:0.2. Comparing the stoichiometries of the mixtures after purification with those of the original ArMs suggests that CoPPIX binds to HasAp by (partly) replacing RuPPIX or ZnPPIX. Because more than one RuPPIX are bound to HasAp, replacing one of the RuPPIX by CoPPIX would produce a new ArM consisting of **RuPPIX-CoPPIX-HasAp**. Replacement of the single ZnPPIX in **ZnPPIX-HasAp** by CoPPIX would produce a new ArM consisting of **CoPPIX-HasAp**.

The apparent dissociation contant (K_D) values for ZnPPIX, RuPPIX and CoPPIX were estimated to be ~0.02 μM for ZnPPIX, ~34 μM for RuPPIX and ~ 0.3 μM for CoPPIX (see Fig. S7 and Table S2). The K_D value of 0.3 μM for CoPPIX confirms that CoPPIX in solution can bind to HasAp. Further evidence for CoPPIX binding to HasAp was found by the increased thermostability of **ZnPPIX-HasAp** and **RuPPIX-HasAp** following titration with CoPPIX. The large error in the estimated K_D value of RuPPIX binding to HasAp may be related to the observed binding ratio of ~2:1 in the RuPPIX-HasAp sample resulting in more complex behaviour that is not well-represented by our fit (Fig. S7B). The relatively high K_D for RuPPIX binding aligns with known properties of Ru-based compounds, which typically require elevated temperatures for efficient binding. To facilitate a comparison of K_D values for the different ligands, titration curves were measured at room temperature, while the RuPPIX-containing ArMs were prepared by overnight incubation at 50 °C, under which conditions the RuPPIX cofactors bind stably to the protein. During the titration reactions 15 % DMF was present, lowering the initial T_i of **ZnPPIX-HasAp** and **RuPPIX-HasAp** to 65 °C and 68 °C. Titrating CoPPIX to **ZnPPIX-HasAp**, an increase in T_i was observed beyond the maximal detection temperature of 95 °C (Fig. S5F) and T_i could only be determined for mixtures of 1:0.1 of **ZnPPIX-HasAp** to

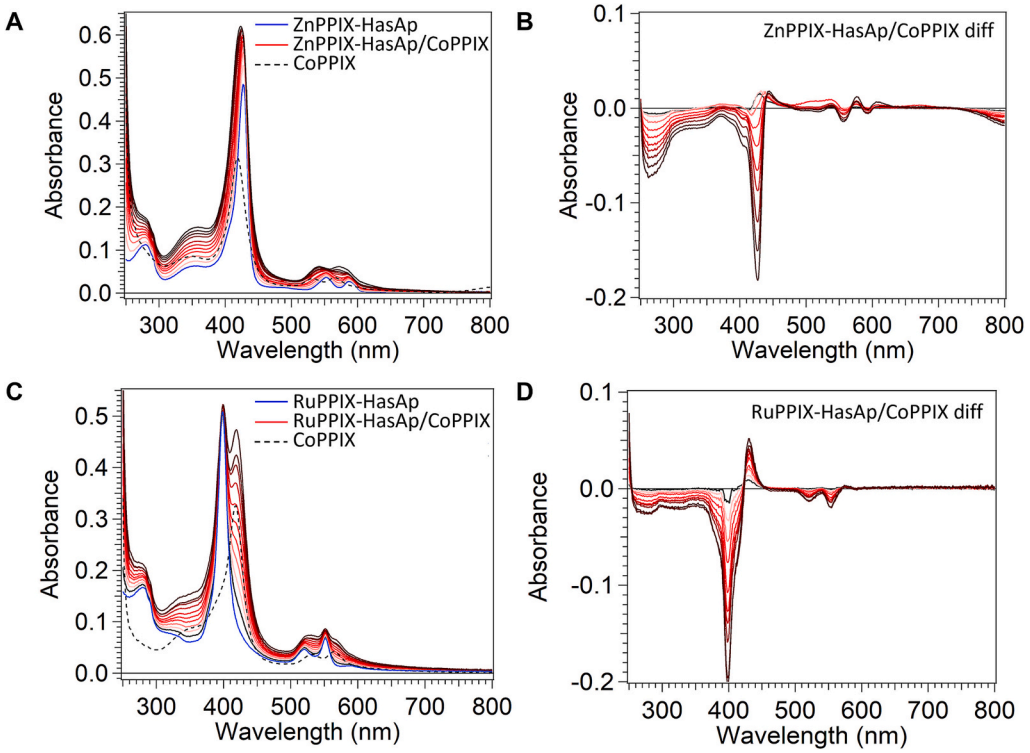

Fig. 2. Titration of CoPPIX to **ZnPPIX-HasAp** (**A**) or **RuPPIX-HasAp** (**C**). Samples contained 0.8 nmol of **ZnPPIX-HasAp** or **RuPPIX-HasAp** in 200 μL 50 mM NaPi pH 8.0 buffer and were titrated with 0.1 mM CoPPIX in DMF, added in 1 μL (0.1 nmol) additions up to 1 nmol total. **B** and **D**: Difference spectra subtracting the individual spectra of CoPPIX and **ZnPPIX-HasAp** (**B**) or CoPPIX and **RuPPIX-HasAp** (**D**) from the absorption spectra of the titration mixtures.

CoPPIX (Fig. S4F). Titrating CoPPIX to **RuPPIX-HasAp** the T_i steadily increased to 80 °C (Fig. S4G, S5G). Finally, the CD spectra of **ZnPPIX-HasAp** and **RuPPIX-HasAp** changed after mixing with CoPPIX, resembling more closely the spectrum of *holo*HasAp (Fig. S6, D and E, yellow curve), which is another indication that the titrated CoPPIX would bind to HasAp.

2.1.3. *Metal coordination and porphyrin binding sites*

The UV–Vis spectra of the ArMs are characteristic of their coordinated metal and are shown in Fig. 3 [49]. The spectral characteristics of ZnPPIX bound to HasAp (Fig. 3B) can be used as an indication of how ZnPPIX is coordinated [31,49]. The bands of **ZnPPIX-HasAp** at 552 nm and 586 nm in Fig. 3B are characteristic of the porphyrin Q bands and their maxima match closely with reported spectra of Zn(II)-protoporphyrin IX dimethyl ester in an aqueous solution of 5 mM 1-methylimidazole [31], indicative of ligation of Zn(*II*)PPIX to a histidine imidazole ring. Haem in the binding pocket of HasAp is coordinated by H32 and Y75 (Fig. 1B). Zn-compounds tend to be penta-coordinated [50] although hexacoordination cannot be excluded.

The Q-bands of **RuPPIX-HasAp** (Fig. 3A) were compared to RuPPIX dissolved in NaPi buffer containing 5 mM imidazole as well as to RuPPIX in NaPi buffer containing 5 % ethanol (Fig. S8, yellow spectrum). The UV–vis spectrum of **RuPPIX-HasAp** was found to be mostly comparable to that of free RuPPIX in imidazole buffer (Fig. S8, green spectrum). The minimal spectral changes in RuPPIX upon binding to HasAp indicate binding in the Ru(II) state. As **RuPPIX-HasAp** binds ~2 RuPPIX *per* HasAp, RuPPIX is bound at different protein locations. The five histidines in HasAp are H32 and H83 in the binding pocket, H74 and H134 near the pocket, and H179 on the other side of the protein. Considering the refolding of HasAp and increased thermostability upon binding of RuPPIX, it is assumed that RuPPIX is bound to H32 in the binding pocket. With RuPPIX bound to H32, steric hindering should prevent the binding of a second RuPPIX to H83, which is very close. In addition, steric hindrance should prevent binding to H134 which is buried in the protein interior. H74 or H179, therefore, are the most likely candidates for binding additional RuPPIX.

Myoglobin coordinates haem only with histidine and a crystal structure of **CoPPIX-Mb** is available (PDB ID 1YOG [47], Fig. 1C) showing coordination to the binding pocket histidine. Compared to free CoPPIX in NaPi buffer containing 4 % DMF (Fig. 3C, red spectrum), the Soret maximum of CoPPIX in **CoPPIX-Mb** (Fig. 3C, black spectrum) shifted from 418 nm to 426 nm and the Q-bands moved from 530 nm and 564 nm to 535 nm and 568 nm. The Soret maximum and two Q-bands are characteristic of Co(*III*)PPIX [51]. The width at half maximum of the CoPPIX Soret band was reduced from 34 nm to 31 nm upon binding to Mb. **CoPPIX-Mb** was found to bind ~3 CoPPIX *per* protein and the exterior site of Mb contains several histidines to which additional CoPPIX may have bound.

In the spectrum of the **RuPPIX-HasAp** mixed with CoPPIX (Fig. 3D, blue spectrum), two Soret bands appeared at 400 nm and 422 nm characteristic for RuPPIX and CoPPIX, respectively, indicating a 4 nm redshift compared to unbound CoPPIX (Fig. 3D, red spectrum). For **ZnPPIX-HasAp** mixed with CoPPIX (Fig. 3E, blue spectrum), one peak was observed with a maximum of 427 nm, however a shoulder on the left side of the spectrum indicated the presence of CoPPIX (see arrow in Fig. 3D). The Soret maxima of mixtures of **RuPPIX-HasAp**/CoPPIX (Fig. 3D, blue spectrum) and **ZnPPIX-HasAp**/CoPPIX (Fig. 3E, blue spectrum) indicate binding of CoPPIX to HasAp, forming Co(*III*)PPIX.

2.1.4. *Photoreduction of MV^{2+} by ZnPPIX-HasAp and RuPPIX-HasAp*

The ability of the HasAp-metalloporphyrin photosensitizer ArMs to reduce MV^{2+} to $MV^{\bullet+}$ was tested by irradiation into the Soret band of **ZnPPIX-HasAp** (irradiated at 435 nm) and **RuPPIX-HasAp** (irradiated at 385 nm) in presence of TEOA as sacrificial donor (SD). The build-up of photoreduced $MV^{\bullet+}$ is presented in Fig. S9 and S10. While the curves suggest that the PS ArMs are capable of photoreducing MV^{2+}, control experiments on irradiated buffer solutions of MV^{2+} and TEOA also show formation of $MV^{\bullet+}$ upon irradiation at 385 nm and a small

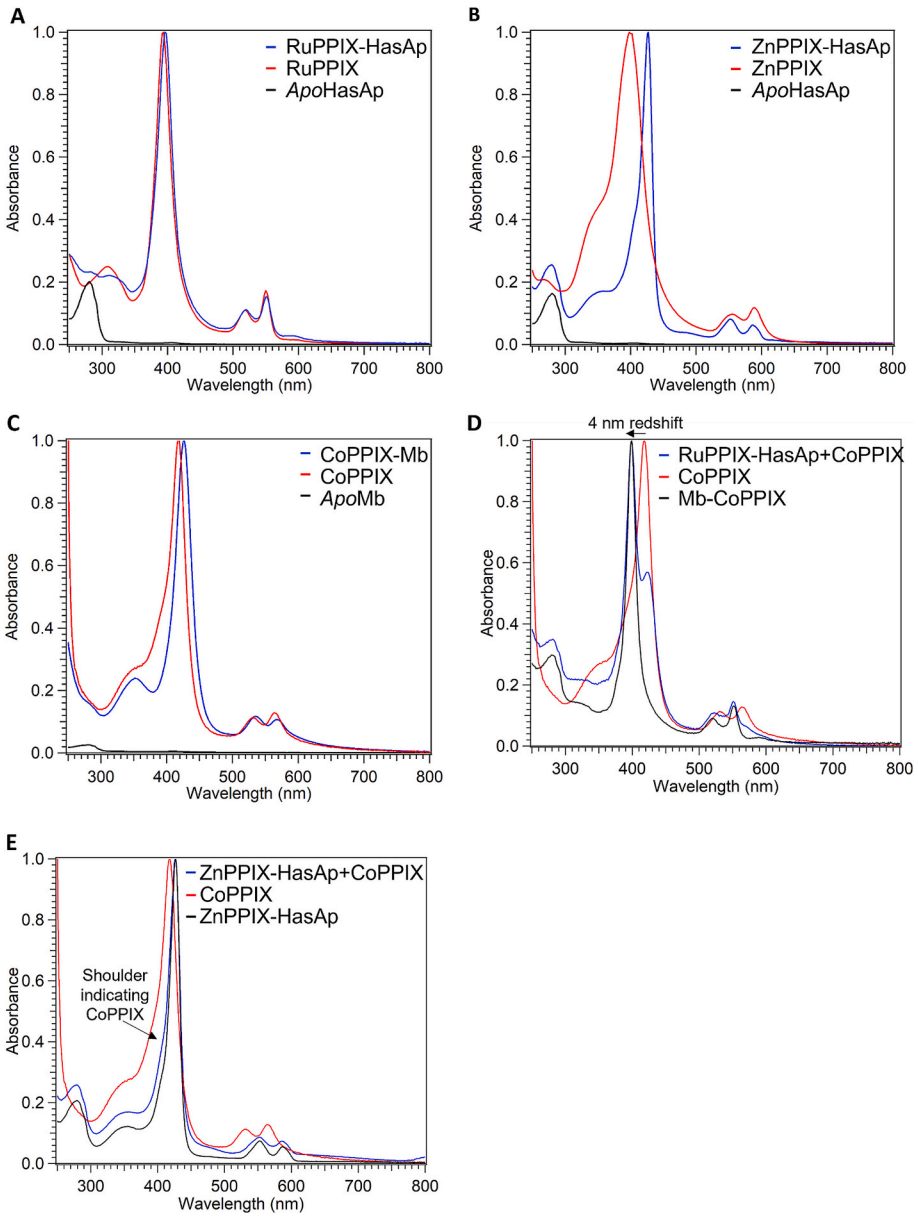

Fig. 3. UV–vis spectra of **RuPPIX-HasAp** (**A**) **ZnPPIX-HasAp** (**B**), **CoPPIX-Mb** (**C**), **RuPPIX-HasAp** mixed with CoPPIX (**D**), and **ZnPPIX-HasAp** mixed with CoPPIX (**E**) (blue spectra). The spectra are compared to the spectra of the free ligands (red spectra). In **A-C** the spectra of the apoprotein are also shown, and in **D** and **E** the spectra of **RuPPIX-HasAp** and **ZnPPIX-HasAp** are shown for comparison (black spectra). All spectra are normalized to their Soret peak. All samples were prepared in 20 mM NaPi, pH 7.0. (For interpretation of the references to colour in this figure legend, the reader is referred to the web version of this article.)

accumulation of $MV^{\bullet+}$ upon irradiation at 435 nm. As laid out in the SI section, an adduct formed by MV^{2+}/TEOA may explain the observed photoreduction of MV^{2+} to $MV^{\bullet+}$ for the MV/TEOA mixtures [52,53]. Fig. 4 shows emission quenching of **ZnPPIX-HasAp** or **RuPPIX-HasAp** in the presence of TEOA upon titration of MV^{2+} (Fig. 4A for a **ZnPPIX-HasAp** and B for **RuPPIX-HasAp**) and the corresponding Stern-Volmer plots (Fig. 4C). The Stern-Volmer constant (K_{SV}) for **ZnPPIX-HasAp** estimated from the fit is $1.5*10^3$ M^{-1} and K_{SV} of **RuPPIX-HasAp** is $16*10^3$ M^{-1}.

The Stern-Volmer constant K_{SV} can be defined as follows:

$$K_{SV} = \tau^* k_q \quad (1)$$

Here τ is the lifetime of the emitting species and k_q the bimolecular rate constant of the quenching reaction. The observed difference in K_{SV} for **ZnPPIX-HasAp** and **RuPPIX-HasAp** could be the result of a difference in the emission lifetimes of the ArMs or in the bimolecular rate constants. The bimolecular rate constant depends on the diffusion speed of the interacting molecules, which is primarily determined by the protein sizes of the ArMs and is expected to be the same for **ZnPPIX-HasAp** and **RuPPIX-HasAp**. To gain insight in the lifetime of the emitting species, Time-Resolved Single Photon Counting (TRSPC) spectroscopy was performed on the ArMs using 442 nm excitation in the Soret band (Fig. S13). The detected lifetimes with the TRSPC instrumentation were in the nanosecond range, which is the expected timescale for excited-state emission, in addition to a non-decaying background signal that represents a phosphorescence signal that decays on timescales exceeding the time window of our instrumentation. Table 2 shows the excited-state lifetimes, and the lifetime traces are presented in Fig. S13. The large amplitude of the phosphorescence background signal for **RuPPIX-HasAp** (Fig. S13B) compared to **ZnPPIX-HasAp** (Fig. S13A) suggests that the emitting species in Eq. (1) had much slower decay for **RuPPIX-HasAp**, providing an explanation for its

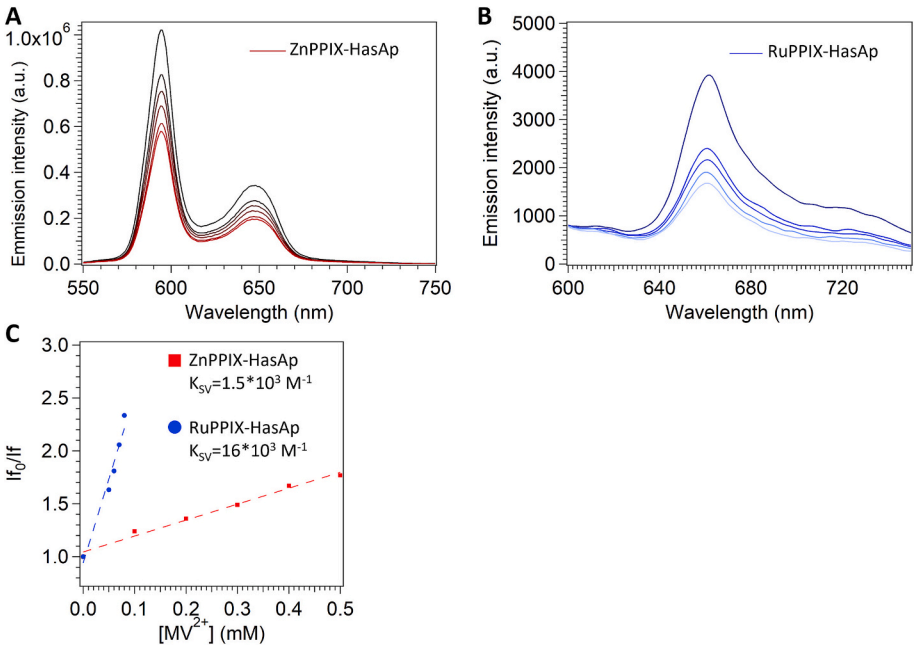

Fig. 4. Emission quenching of **ZnPPIX-HasAp** (red) and **RuPPIX-HasAp** (blue) by MV^{2+}. **A** Emission spectrum of 5.0 μM **ZnPPIX-HasAp** (red, excitation 435 nm) and **B** 3.0 μM **RuPPIX-HasAp** (blue, excitation 385 nm) with titration of respectively 0–0.5 mM and 0–0.08 mM $MVCl_2$ (dark to light spectra). **C** Stern-Volmer plot of the data shown in **A** and **B** with data of **RuPPIX-HasAp** in blue circles and of **ZnPPIX-HasAp** in red squares. Buffer solutions contained 100 mM NaPi, pH 8.4 and 0.1 M TEOA. The respective Stern-Volmer constants (K_{SV}) are shown in **C.** (For interpretation of the references to colour in this figure legend, the reader is referred to the web version of this article.)

Table 2
Fluorescence lifetimes and fractional amplitudes of the ArMs and porphyrins (excitation at 442 nm). Buffer solution contained 50 mM NaPi, pH 8.0.*Purified to remove free porphyrins.

Sample	τ_1 (ns)	A_1 (%)	τ_2 (ns)	A_2 (%)	τ_3 (ns)	A_3 (%)	$<\tau>$ (ns)
ZnPPIX-HasAp	2.1 ± 0.01	56.3	1.3 ± 0.03	29.0	0.09 ± 0.03 0.03	14.7	1.6
RuPPIX-HasAp	2.9 ± 0.3	37.5	0.57 ± 0.05	62.5			1.4
RuPPIX-HasAp / CoPPIX*	6.2 ± 0.9	n.d.	2.7 ± 0.1	n.d.	<< 0.03	n.d.	n.d.
ZnPPIX-HasAp / CoPPIX*	0.8 ± 0.02	12.2	2.0 ± 0 0.05	87.9			1.7

larger K_{SV}. The sample of **RuPPIX-HasAp**/CoPPIX displayed ultrafast quenching within the instrument response time, in addition to two minor fractions that decay in the ns range. We suspect that for those samples, co-bound CoPPIX may quench the RuPPIX excited states via intra-protein electron transfer from RuPPIX to CoPPIX.

2.2. Hydrogen evolution activity

2.2.1. Photocatalytic activity of ZnPPIX-HasAp mixed with CoPPIX-Mb or CoPPIX

The ability of the full systems to photosensitize hydrogen evolution was tested using TEOA as the sacrificial donor and MV^{2+} as the electron relay. Hydrogen evolution experiments were carried out by continuous irradiation of degassed solutions in the presence of 95 mM TEOA and 0.25 or 0.5 mM $MVCl_2$ (in the form of $C_{12}H_{14}N_2Cl_2{\bullet}xH_2O$) in 50 mM NaPi buffer, pH 8.0 as described in the SI section. Concentrations in terms of the porphyrin ligands were 5.0 μM ZnPPIX or 4.7 μM RuPPIX and 1.6 μM CoPPIX. For irradiation of ZnPPIX-containing samples a 435 nm LED was used with an output of 11.5 ± 0.5 mW.

Figs. 5 and 6 present the hydrogen evolution activities. Each photocatalytic experiment discussed below was realised at least twice with the average curves shown and the standard error is indicated. Moderate hydrogen was produced by mixtures of **ZnPPIX-HasAp**/CoPPIX (Fig. 5A, blue trace) or mixtures of **ZnPPIX-HasAp/CoPPIX-Mb** (Fig. 5A, black trace) under 435 nm irradiation. Hydrogen was produced with similar rates for the first 800 min (~0.7 mmol H_2, turnover number, *TON*, of ~120), after which mixtures with CoPPIX outperformed those with **CoPPIX-Mb**. In the protein-free system consisting of ZnPPIX and CoPPIX in the presence of MV^{2+} and TEOA (Fig. S17C, blue trace), no significant hydrogen production was observed, this was expected to be related to the poor solubility or aggregation of the porphyrins in aqueous solution. No hydrogen was produced in dark (Fig. 5A, red trace), or in solutions with only ZnPPIX-HasAp, MV^{2+} and TEOA (Fig. 5A, yellow trace). In absence of MV^{2+} very limited hydrogen evolved, likely because of kinetic limitations (Fig. S17A). Because analysis of **ZnPPIX-HasAp**/CoPPIX mixtures indicated that CoPPIX would bind to HasAp, we performed additional experiments on samples that were subjected to a column purification step prior to the photocatalysis experiment, removing unbound or loosely bound porphyrins. Hereto **ZnPPIX-HasAp**/CoPPIX mixtures were incubated at room temperature for 30 min after which free porphyrin was removed by reconcentrating 5 times in a 3 kDa cut-off concentrator with 50 mM NaPi pH 8.0 buffer. The purified samples produced similar amounts of hydrogen as the samples without purification (Fig. 5B), indicating that the photo catalytic reaction was driven by **ZnPPIX-HasAp** interacting with protein-bound CoPPIX (in the form of CoPPIX-HasAp) rather than with free CoPPIX. Experiments were halted after 2500 min or irradiation, in which a *TON* of ~349 was reached and activity was still ongoing.

2.2.2. Photocatalytic activity of RuPPIX-HasAp mixed with CoPPIX-Mb or CoPPIX

For irradiation of samples containing RuPPIX, a 385 nm LED was

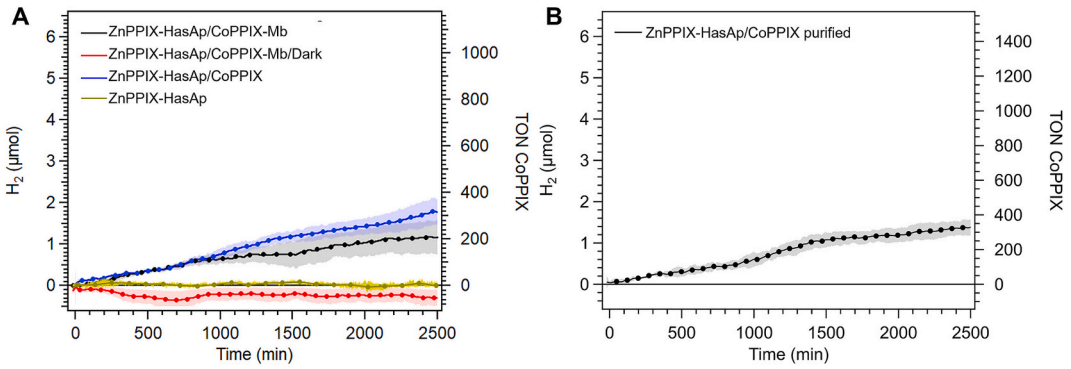

Fig. 5. Hydrogen evolution activity of the ArM systems in the presence of MV^{2+} and TEOA with 435 nm (11.5 ± 0.5 mW LED) irradiation. **A.** Hydrogen evolution by **ZnPPIX-HasAp/CoPPIX-Mb** (black) compared to **ZnPPIX-HasAp**/CoPPIX (blue), **ZnPPIX-HasAp/CoPPIX-Mb** kept dark (red) and solution of **ZnPPIX-HasAp**, lacking **CoPPIX or CoPPIX-Mb** (yellow). **B.** Hydrogen evolution by **ZnPPIX-HasAp**/CoPPIX mixtures purified from free porphyrins prior to photo catalysis. Each curve is the average of at least 2 experiments (standard error in light colour). (For interpretation of the references to colour in this figure legend, the reader is referred to the web version of this article.)

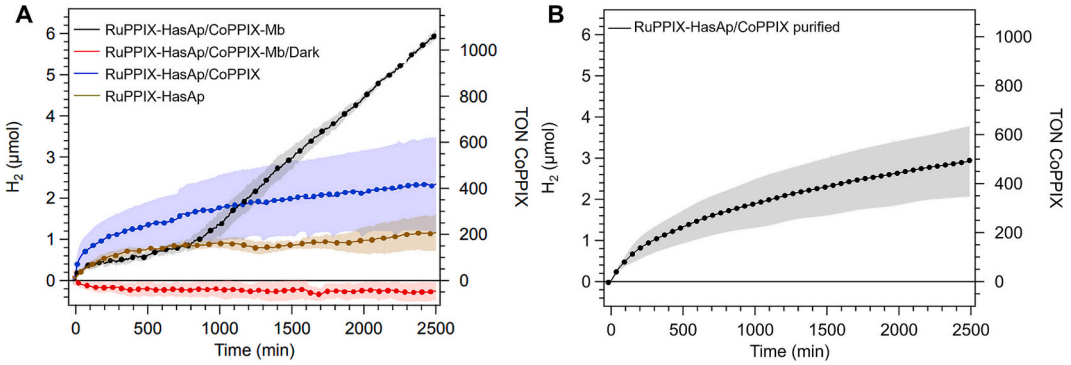

Fig. 6. Hydrogen evolution activity of the ArM systems in the presence of MV^{2+} and TEOA with 385 nm (21 ± 2 mW LED) irradiation. **A.** Hydrogen evolution by **RuPPIX-HasAp/CoPPIX-Mb** (grey) compared to **RuPPIX-HasAp**/CoPPIX (blue), **RuPPIX-HasAp/CoPPIX-Mb** kept dark (red), and **RuPPIX-HasAp** (yellow). **B.** Hydrogen evolution by **RuPPIX-HasAp**/CoPPIX mixtures purified prior to photo catalysis for removal of free porphyrins. Each curve is the average of at least 2 experiments (standard error in light colour). (For interpretation of the references to colour in this figure legend, the reader is referred to the web version of this article.)

used with an output of 21 ± 2 mW. The photon flux was determined using ferrioxalate actinometry (Fig. S15) and was 2.93 μmol/s. Mixtures of **RuPPIX-HasAp/CoPPIX-Mb** or **RuPPIX-HasAp**/CoPPIX were irradiated with 385 nm in the presence of MV^{2+} and TEOA (Fig. 6A). Because 385 nm-irradiation caused photoreduction of MV^{2+} in the presence of TEOA, which possibly formed a charge-transfer complex as discussed below, background activity was observed in mixtures of MV^{2+} and TEOA alone (Fig. S17B, red trace) and in mixture of **RuPPIX-HasAp** in the presence of MV^{2+} and TEOA (Fig. 6A, yellow trace), lacking CoPPIX or **CoPPIX-Mb**. The background activity was lower when RuPPIX-HasAp was added to MV^{2+}/TEOA, likely due to the absorbance of the light by RuPPIX-HasAp rather than the putative MV^{2+}/TEOA complex (Fig. 6A, yellow trace). During the first 800 min of activity of the **RuPPIX-HasAp/CoPPIX-Mb** system in the presence of MV^{2+} and TEOA did not exceed the background activity of MV^{2+} and TEOA alone (Fig. S17B, red trace) or of controls with protein-free mixtures of RuPPIX and CoPPIX in the presence of MV^{2+} and TEOA (Fig. S17D, blue trace). In contrast, the mixtures of **RuPPIX-HasAp**/CoPPIX produced hydrogen with a significantly higher rate (Fig. 6A, blue trace). We also performed photocatalysis experiments on **RuPPIX-HasAp**/CoPPIX mixtures that had been subjected to purification. Prior to photocatalysis experiments, **RuPPIX-HasAp**/CoPPIX mixtures were incubated at room temperature for 30 min after which free or loosely bound porphyrin was removed by reconcentrating 5 times in a 3 kDa cut-off concentrator with 50 mM NaPi pH 8.0 buffer. The purified **RuPPIX-HasAp**/CoPPIX mixtures had improved hydrogen evolution activity, and the maximal turnover frequency (TOF_{max}) was increased (Fig. 6B and Table 3).

After ~800 min, a breakpoint was observed for the mixture containing **RuPPIX-HasAp/CoPPIX-Mb** and hydrogen was produced at a much faster rate (Fig. 6A, black trace). As will be explained below, at that stage we observed disappearance from solution of Mb, suggesting

Table 3
*Turnover numbers (*TON*) and turnover frequencies (TOF_{max}) for hydrogen produced* per CoPPIX by irradiation of the different ArM systems in presence of MV^{2+} and TEOA. The turnover frequencies for photon to electron are represented by $pTOF_{max}$.*Purified to remove free porphyrins prior to photocatalysis experiments.

Sample	λ_{irrad} (nm)	*TON* (2500 min)	TOF_{max} (min^{-1})	$pTOF_{max}$ (min^{-1})
ZnPPIX-HasAp/CoPPIX-Mb	435	212	0.14	0.086
RuPPIX-HasAp/CoPPIX-Mb	385	1069	0.6	0.42
ZnPPIX-HasAp/CoPPIX*	435	349	0.2	0.12
RuPPIX-HasAp/CoPPIX*	385	492	1.0	0.70

that this ArM system was destabilized and loss of CoPPIX occurred. In contrast, the activity of **RuPPIX-HasAp**/CoPPIX solutions slowed down at longer timescales (Fig. 6A, blue trace and Fig. 6B). The *TON* (at 2500 min), and *TOF* values of the different systems are presented in Table 3.

2.3. Photostability of the ArMs

For efficient use of ArMs for driving photocatalytic reactions, photostability of the designed artificial metalloproteins is a crucial factor. Several tests were performed as detailed below to check the stability of the HasAp and Mb proteins as well as of the protein-metal porphyrin interaction in photocatalytic conditions. Irradiated samples were purified by reconcentration to remove small molecules, e.g., unbound cofactors, TEOA, and MV^{2+}. No free pigments were observed by UV–Vis spectroscopy of the flow-through that came through the filters of the concentrators during purification (*data not shown*).

2.3.1. Protein stability

To investigate protein stabilities, the ArMs were subjected to gel electrophoresis before and after photocatalysis (see Fig. S18). The gel bands showed that majority of the HasAp protein remained intact during 2500 min irradiation, except for samples of **RuPPIX-HasAp**/CoPPIX, although minor fractions of cleavage products could be seen as lower weight bands (the most prominent indicated with arrows on the gel images in Fig. S18). In contrast, the band of Mb was no longer visible on gel after 2500 min of irradiation at 385 nm or 435 nm. Since two kinetic phases were observed for hydrogen production by **RuPPIX-HasAp**/**CoPPIX-Mb**, samples were also collected around this turning point i.e. after 730 and 1000 min of irradiation. For those samples, a band of Mb, in addition to the band of HasAp, was visible on SDS gel together with some cleavage products (Fig. S18C). This indicated that most of the Mb had remained intact, and that (photo)decomposition occurred at a later stage, correlating with the change in the kinetics of hydrogen generation. **RuPPIX-HasAp**/**CoPPIX-Mb** samples collected at different time points after irradiation were subjected to UV–Vis spectroscopy (Fig. S19C and E) as will be discussed below. The UV-VIS spectra show a decrease of porphyrin signals at longer irradiation times, correlating with disappearance of Mb from solution.

Dynamic light scattering (DLS) performed on the samples after 2500 min irradiation excluded formation of larger particles in solution, such as protein aggregates of metal nanoparticles exceeding the size of the proteins (Fig. S20). DLS is not very sensitive for detection of small oligomers and size-exclusion chromatography multi-angle light scattering (SEC-MALS) was performed (Fig. S21) for further characterization of the protein states. After 2500 min irradiation all samples contained protein monomers with a minor population of dimer (band at ~14.5 mL) and no contributions of higher oligomers were detected. Elution profiles detected at different absorption wavelengths showed that porphyrin cofactors, absorbing at 400 or 426 nm, co-eluted with the protein band detected at 280 nm, showing the presence of protein-bound cofactors. The SEC-MALS did not detect any additional peaks of the cofactors, which would have shown in case of small metal nanoparticles.

2.3.2. Cofactor stability

After the photocatalysis experiments, samples were reconcentrated in a 3 kDa cut-off concentrator, removing free and loosely bound porphyrins and subjected to ICP-MS. Table S6 shows the loss of cofactors comparing Co, Zn and Ru metal intensities before and after 2500 min of photocatalysis (irradiation at 435 nm for ZnPPIX and at 385 nm for RuPPIX). The mixtures containing **CoPPIX-Mb** showed the largest losses after 2500 min irradiation and reconcentration, suggesting that most of the cofactors were removed or loosely bound to the proteins after the experiment. In this sample, Mb was not visible on gel anymore after 2500 min irradiation (Fig. S18A) indicating its precipitation from solution. Because the kinetics of photo activity of the mixture **RuPPIX-HasAp**/**CoPPIX-Mb** had a turning point around ~800 min (Fig. 6A, black curve), samples were also analysed after shorter irradiation periods (730 or 1000 min of 385-nm irradiation). Gel images of those samples (Fig. S18C) showed a band of HasAp and Mb in addition to some cleavage bands, indicating that majority of protein cleavage or precipitation occurred at longer irradiation times. In the mixture of **RuPPIX-HasAp**/CoPPIX, purified from free porphyrins prior to photo catalysis, ~40 % of the Ru and Co cofactors that were originally present in the sample remained after 2500 min irradiation and re-purification (Table S6). Gel electrophoresis of these mixtures showed that about half of the HasAp was cleaved after 2500 min irradiation (Fig. S18B), so that cofactor losses in this sample could be due to protein cleavage. Since analysis of the **RuPPIX-HasAp**/**CoPPIX-Mb** mixtures indicated that most of the HasAp was intact after 730 or 1000 min, we suspect that HasAp cleavage at prolonged 385-nm irradiation occurred on timescales >1000 min. No cofactor losses were observed in ICP-MS of **ZnPPIX-HasAp**/CoPPIX mixtures that were purified from free porphyrins prior to photocatalysis experiments. ICP-MS (Table S6) and protein analysis (Fig. S18B) shows that the HasAp protein remained intact after 2500 min of 435-nm irradiation.

UV-VIS spectra were collected of the samples before and after photocatalysis experiments (Fig. S19). After the irradiation experiments samples were reconcentrated in a 3 kDa cut-off concentrator, removing free or loosely bound cofactors prior to UV-VIS spectroscopy. The **ZnPPIX-HasAp**/CoPPIX mixture showed moderate cofactor bleaching after 2500 min irradiation (Fig. S19B). In the spectrum of **RuPPIX-HasAp**/CoPPIX, bleaching of the RuPPIX band was observed relative to CoPPIX (Fig. S19A). The mixtures containing **CoPPIX-Mb** showed the strongest bleaching of the cofactor signals (Fig. S19C and D), which agrees with the loss of cofactors for these samples observed via ICP-MS (Table S6), while UV-VIS spectra collected after 730 and 1000 min of 385-nm irradiation (Fig. S19E) had ~50 % cofactor bleaching.

3. Discussion

The goal of this study was to combine porphyrin-based PS and HEC ArMs for light-driven hydrogen production via inter- or intra-protein electron transfer —a concept that has been less explored than photocatalysis using HEC ArMs in solutions with a high excess of PS molecules. The results show that our ArM mixtures, with a PS to HEC ratio of 3–4, successfully produced hydrogen in the presence of MV and TEOA. The abundant-metal ArM system based on **ZnPPIX-HasAp** and **CoPPIX-Mb** produced hydrogen with a *TON* (2500 min) of ~200 that could be increased to a *TON* of ~350 by replacing **CoPPIX-Mb** with CoPPIX (Fig. 5, Table 3), likely due to the instability of the Mb protein scaffold at longer timescales. CD, UV-VIS spectroscopy, and thermo analysis of **ZnPPIX-HasAp**/CoPPIX mixtures indicated that CoPPIX would bind to the HasAp ArMs, implying that a mixture of **ZnPPIX-HasAp**/**CoPPIX-HasAp** had formed that was more active in hydrogen production than the **ZnPPIX-HasAp**/**CoPPIX-Mb** system. No activity was observed for protein-free mixtures of ZnPPIX and CoPPIX in the presence of MV^{2+} and TEOA (Fig. S17C, blue trace), while similar activity was observed for **ZnPPIX-HasAp**/CoPPIX mixtures purified from free porphyrins (comparing Fig. 5A, blue trace and Fig. 5B), supporting the notion that the active catalyst consisted of protein-bound CoPPIX. The performances of the **ZnPPIX-HasAp**/**CoPPIX-Mb** and **ZnPPIX-HasAp**/CoPPIX systems are comparable to those in previous studies on CoPPIX-Mb [12,13], in which *TONs* ranging from 234 to 518 depending on pH conditions and hydrogen production up to ~0.5 μmol were reported, and to the activity of CoPPIX-cytochrome b_{562} in a sealed reactor cuvette, for which a *TON* of 125 was reported. For CoPPIX-containing peptide-based systems higher *TONs* have been reported, ranging from 606 to 2390 for with a small peptide chain, depending on the catalyst concentration [54]. At high concentrations, peptide aggregation was reported that limited the activity. Furthermore, for a cobalt deuteroporphyrin-binding mini-protein with a more enveloping side chain, an increased *TON* of 10,000 was reported, and a lifetime of 40 h [17]. A key distinction in our study is the

incorporation of the PS into a protein scaffold, increasing the stability of the PS, and consequently the lower ratio of PS to catalyst that was used. In the referred studies, a 0.35–1 mM concentration of $Ru(bpy)_3Cl_2$ was used with 0.1–5 μM of catalyst, resulting in a PS-to-catalyst excess ranging from 175- to 3500-fold. In contrast, our study employed approximately 5 μM of an earth-abundant photosensitizer, in the form of ZnPPIX-HasAp, which corresponds to only a 3–4-fold excess of PS relative to the CoPPIX or CoPPIX-Mb catalyst. The lifetime for activity of the **ZnPPIX-HasAp**/CoPPIX system exceeded those previously reported for CoPPIX-binding artificial enzymes in the presence of $Ru(bpy)_3Cl_2$, which photo decomposition over time often is a limiting factor for photocatalytic efficiency. The **ZnPPIX-HasAp**/CoPPIX system remained active for 42 h and no loss of cofactors and only mild protein cleavage was observed after 2500 min of 435 nm irradiation.

RuPPIX-containing mixtures required irradiation at 385 nm for photosensitizing, at which illumination wavelength background photo activity was observed of MV^{2+}/TEOA solutions with and without RuPPIX-HasAp (Fig. 6A, yellow trace and fig. S17B red trace). As mentioned in the Materials and Methods of the SI section, a MV^{2+}/TEOA charge transfer complex may have been formed that could be photo activated by 385 nm illumination [52,53]. A potential explanation for how the formation of $MV^{\bullet+}$ leads to hydrogen-generation was proposed by Bauer et al. 1992 [55], who suggest the formation of a protonated radical $MVH^{+\bullet}$ species, capable of reacting with a second $MVH^{+\bullet}$ moiety to release hydrogen. The **RuPPIX-HasAp**/CoPPIX system purified from free porphyrins contained HasAp-bound CoPPIX, in the form of RuPPIX-CoPPIX-HasAp, and produced hydrogen with an activity distinctive from the background activity of MV^{2+}/TEOA, reaching a *TON* (2500 min) of ~500 corresponding to ~3.5 μmol of H_2. Compared to the other samples, this system had the highest TOF_{max} (Table 3). The activity of the **RuPPIX-HasAp**/CoPPIX mixtures would gradually slow down, likely because of HasAp protein cleavage at prolonged exposure to UV irradiation (Fig. S18). Mixtures without MV^{2+} produced very little hydrogen (Fig. S17B, blue curve), even though the HasAp ArMs contained both RuPPIX and CoPPIX. The observation of ultrafast Ru excited-state quenching in this sample suggests that light-induced intra-protein electron transfer to CoPPIX occurs. However, electron back transfer and rapid charge recombination processes may have hindered the efficient catalysis via intra-protein electron transfer to CoPPIX.

For the **RuPPIX-HasAp**/**CoPPIX-Mb** system a steep increase in activity was observed after ~800 min of photocatalysis, reaching exceptional activity with a *TON* of 1069 after 2500 min of 385 nm-irradiation (Fig. 6A, Table 3). The marked change in the hydrogen production rate signifies a change in the active species. Analyses of the samples after 2500 min photocatalysis did not detect Mb but some CoPPIX was detected. Results from ICP-MS and SEC-MALS (Table S6, Fig. S21) suggested that some CoPPIX was rebound to HasAp and co-eluted with protein, while overall cofactor-protein interactions were destabilized. As the performance of this sample differed from that of **RuPPIX-HasAp**/CoPPIX, the nature of the gradually formed active species in this system remains to be resolved.

4. Conclusions

In this work, we aimed to design porphyrin-based PS artificial metalloproteins (ArMs) and develop a fully protein-based system in solution, establishing light-driven electron transfer from the PS ArMs to co-mixed hydrogen-evolution catalyst ArMs via an electron mediator. HasAp-metal porphyrin ArMs were characterized and tested for their ability to photosensitize hydrogen evolution, catalysed by CoPPIX or CoPPIX-Mb in the presence of TEOA as a sacrificial donor and MV^{2+} as an electron relay. We found that free CoPPIX could bind to HasAp ArMs partly through exchange with ZnPPIX or RuPPIX. The resulting HasAp-based systems demonstrated greater stability in hydrogen production than mixtures containing CoPPIX-Mb, in which Mb gradually disappeared, likely due to precipitation or cleavage. Detailed analysis of the irradiated systems revealed that HasAp-based ArMs with ZnPPIX and CoPPIX remained intact after 2500 min (~42 h) of irradiation, showing only minor signs of protein cleavage. In contrast, the ruthenium-containing systems exhibited higher activity but required UV irradiation, with analysis after photocatalysis revealing cleavage products. This work demonstrates that photocatalytic hydrogen production can be achieved in aqueous solutions through inter-protein electron transfer between photosensitizer and catalyst ArMs, mediated by an electron carrier. HasAp provides a stable scaffold for binding porphyrin metal complexes, which are highly effective for both photosensitization and photocatalysis. With this concept established, further optimization of the design for photosensitizing and hydrogen-generating catalytic ArMs, electron mediators, and buffer conditions could enhance photocatalytic performance.

Funding

This research did not receive any specific grant from funding agencies in the public, commercial, or not-for-profit sectors.

CRediT authorship contribution statement

L.V. Opdam: Writing – review & editing, Writing – original draft, Visualization, Methodology, Investigation, Data curation, Conceptualization. **S.K. Goetzfried:** Investigation. **E. Polanco:** Methodology, Investigation. **S. Bonnet:** Writing – review & editing, Supervision. **A. Pandit:** Writing – review & editing, Writing – original draft, Supervision, Project administration, Conceptualization.

Declaration of competing interest

The authors declare that they have no known competing financial interests or personal relationships that could have appeared to influence the work reported in this paper.

Acknowledgements

We thank Dr. S. Zheng for the ICP-MS measurements, A. J. Cramer-Blok for measurement of the SEC-MALS spectra, and Ing. S. G. Romeijn for the training on the fluorescence spectrophotometer.

Appendix A. Supplementary data

Supplementary data to this article can be found online at https://doi.org/10.1016/j.jinorgbio.2025.112855.

Data availability

Data will be made available on request.

References

[1] S. Solomon, G.K. Plattner, R. Knutti, P. Friedlingstein, Irreversible climate change due to carbon dioxide emissions, Proc. Natl. Acad. Sci. 106 (6) (2009) 1704–1709.
[2] A.L. Hammond, Solar energy: the largest resource, Science 177 (4054) (1972) 1088–1090.
[3] V. Balzani, L. Moggi, M. Manfrin, F. Bolletta, M. Gleria, Solar energy conversion by water photodissociation: transition metal complexes can provide low-energy cyclic systems for catalytic photodissociation of water, Science 189 (4206) (1975) 852–856.
[4] J. Dawson, Prospects for hydrogen as an energy resource, Nature 249 (5459) (1974) 724–726.
[5] P.T. Aakko-Saksa, C. Cook, J. Kiviaho, T. Repo, Liquid organic hydrogen carriers for transportation and storing of renewable energy–review and discussion, J. Power Sources 396 (2018) 803–823.
[6] H. Hennig, Homogeneous photo catalysis by transition metal complexes, Coord. Chem. Rev. 182 (1) (1999) 101–123.
[7] N. Hoffmann, Homogeneous photocatalytic reactions with organometallic and coordination compounds—perspectives for sustainable chemistry, ChemSusChem 5 (2) (2012) 352–371.

[8] K. Ladomenou, M. Natali, E. Iengo, G. Charalampidis, F. Scandola, A. G. Coutsolelos, Photochemical hydrogen generation with porphyrin-based systems, Coord. Chem. Rev. 304 (2015) 38–54.
[9] T. Nakazono, A.R. Parent, K. Sakai, Cobalt porphyrins as homogeneous catalysts for water oxidation, Chem. Commun. 49 (56) (2013) 6325–6327.
[10] D. Wang, J.T. Groves, Efficient water oxidation catalyzed by homogeneous cationic cobalt porphyrins with critical roles for the buffer base, Proc. Natl. Acad. Sci. 110 (39) (2013) 15579–15584.
[11] J.P. Collman, P.S. Wagenknecht, N.S. Lewis, Hydride transfer and dihydrogen elimination from osmium and ruthenium metalloporphyrin hydrides: model processes for hydrogenase enzymes and the hydrogen electrode reaction, J. Am. Chem. Soc. 114 (14) (1992) 5665–5673.
[12] D.J. Sommer, M.D. Vaughn, G. Ghirlanda, Protein secondary-shell interactions enhance the photoinduced hydrogen production of cobalt protoporphyrin IX, Chem. Commun. 50 (100) (2014) 15852–15855.
[13] D.J. Sommer, M.D. Vaughn, B.C. Clark, J. Tomlin, A. Roy, G. Ghirlanda, Reengineering cyt b562 for hydrogen production: a facile route to artificial hydrogenases, Biochim. Biophys. Acta Bioenerg. 1857 (5) (2016) 598–603.
[14] T.D. Rapson, H. Ju, P. Marshall, R. Devilla, C.J. Jackson, S. Giddey, et al., Engineering a solid-state metalloprotein hydrogen evolution catalyst, Sci. Rep. 10 (1) (2020) 3774.
[15] J.M. Le, K.L. Bren, Engineered enzymes and bioinspired catalysts for energy conversion, ACS Energy Lett. 4 (9) (2019) 2168–2180.
[16] M. Bacchi, E. Veinberg, M.J. Field, J. Niklas, T. Matsui, D.M. Tiede, et al., Artificial hydrogenases based on cobaloximes and heme oxygenase, ChemPlusChem 81 (10) (2016) 1083–1089.
[17] E.H. Edwards, J.M. Le, A.A. Salamatian, N.L. Peluso, L. Leone, A. Lombardi, et al., A cobalt mimochrome for photochemical hydrogen evolution from neutral water, J. Inorg. Biochem. 230 (2022) 111753.
[18] V. Firpo, J.M. Le, V. Pavone, A. Lombardi, K.L. Bren, Hydrogen evolution from water catalyzed by cobalt-mimochrome VI* a, a synthetic mini-protein, Chem. Sci. 9 (45) (2018) 8582–8589.
[19] A. Juris, V. Balzani, F. Barigelletti, S. Campagna, P. Belser, l, von Zelewsky A von., Ru (II) polypyridine complexes: photophysics, photochemistry, eletrochemistry, and chemiluminescence, Coord. Chem. Rev. 84 (1988) 85–277.
[20] M. Joseph, S. Haridas, Recent progresses in porphyrin assisted hydrogen evolution, Int. J. Hydrog. Energy 45 (21) (2020) 11954–11975.
[21] K. Kalyanasundaram, Photochemistry and sensitized evolution of hydrogen from water using water-soluble cationic porphyrins. Tetrakis (trimethylaminophenyl) porphyrinatozinc and its free base, J. Chem. Soc. Farad. Trans. 2 Mol. Chem. Phys. 79 (9) (1983) 1365–1374.
[22] A.C. Ghosh, C. Duboc, M. Gennari, Synergy between metals for small molecule activation: enzymes and bio-inspired complexes, Coord. Chem. Rev. 428 (2021) 213606.
[23] A. Vaidyalingam, P.K. Dutta, Analysis of the photodecomposition products of Ru (bpy) 32+ in various buffers and upon zeolite encapsulation, Anal. Chem. 72 (21) (2000) 5219–5224.
[24] J.S. O'Neill, L. Kearney, M.P. Brandon, M.T. Pryce, Design components of porphyrin-based photocatalytic hydrogen evolution systems: a review, Coord. Chem. Rev. 467 (2022) 214599.
[25] M. Tahoun, C.T. Gee, V.E. McCoy, P.M. Sander, C.E. Müller, Chemistry of porphyrins in fossil plants and animals, RSC Adv. 11 (13) (2021) 7552–7563.
[26] S.C. Silver, J. Niklas, P. Du, O.G. Poluektov, D.M. Tiede, L.M. Utschig, Protein delivery of a Ni catalyst to photosystem I for light-driven hydrogen production, J. Am. Chem. Soc. 135 (36) (2013) 13246–13249.
[27] S.R. Soltau, J. Niklas, P.D. Dahlberg, K.L. Mulfort, O.G. Poluektov, L.M. Utschig, Charge separation related to photocatalytic H2 production from a Ru–Apoflavodoxin–Ni biohybrid, ACS Energy Lett. 2 (1) (2017) 230–237.
[28] U. Brahmachari, P.R. Pokkuluri, D.M. Tiede, J. Niklas, O.G. Poluektov, K. L. Mulfort, et al., Interprotein electron transfer biohybrid system for photocatalytic H 2 production, Photosynth. Res. 143 (2020) 183–192.
[29] K. Oohora, A. Onoda, T. Hayashi, Hemoproteins reconstituted with artificial metal complexes as biohybrid catalysts, Acc. Chem. Res. 52 (4) (2019) 945–954.
[30] O. Horváth, Z. Valicsek, M.A. Fodor, M.M. Major, M. Imran, G. Grampp, et al., Visible light-driven photophysics and photochemistry of water-soluble metalloporphyrins, Coord. Chem. Rev. 325 (2016) 59–66.
[31] T. Komatsu, R.M. Wang, P.A. Zunszain, S. Curry, E. Tsuchida, Photosensitized reduction of water to hydrogen using human serum albumin complexed with zinc–Protoporphyrin IX, J. Am. Chem. Soc. 128 (50) (2006) 16297–16301.
[32] E.R. Clark, D.M. Kurtz, Photosensitized H 2 generation from "one-pot" and "two-pot" assemblies of a zinc-porphyrin/platinum nanoparticle/protein scaffold, Dalton Trans. 45 (2) (2016) 630–638.
[33] P. Ascenzi, A. Bocedi, P. Visca, F. Altruda, E. Tolosano, T. Beringhelli, et al., Hemoglobin and heme scavenging, IUBMB Life 57 (11) (2005) 749–759.
[34] C. Ratledge, L.G. Dover, Iron metabolism in pathogenic bacteria, Ann. Rev. Microbiol. 54 (1) (2000) 881–941.
[35] S. Letoffe, J. Ghigo, C. Wandersman, Iron acquisition from heme and hemoglobin by a *Serratia marcescens* extracellular protein, Proc. Natl. Acad. Sci. 91 (21) (1994) 9876–9880.
[36] I. Stojiljkovic, D. Perkins-Balding, Processing of heme and heme-containing proteins by bacteria, DNA Cell Biol. 21 (4) (2002) 281–295.
[37] G. Centola, D.J. Deredge, K. Hom, Y. Ai, A.T. Dent, F. Xue, et al., Gallium (III)–salophen as a dual inhibitor of *Pseudomonas aeruginosa* heme sensing and iron acquisition, ACS Infect. Dis. 6 (8) (2020) 2073–2085.
[38] G. Jepkorir, J.C. Rodríguez, H. Rui, W. Im, S. Lovell, K.P. Battaile, et al., Structural, NMR spectroscopic, and computational investigation of hemin loading in the hemophore HasAp from *Pseudomonas aeruginosa*, J. Am. Chem. Soc. 132 (28) (2010) 9857–9872.
[39] L.V. Opdam, E.A. Polanco, B. de Regt, N. Lambertina, C. Bakker, S. Bonnet, et al., A screening method for binding synthetic metallo-complexes to haem proteins, Anal. Biochem. 653 (2022) 114788.
[40] C. Shirataki, O. Shoji, M. Terada, S. Ozaki, H. Sugimoto, Y. Shiro, et al., Inhibition of heme uptake in *Pseudomonas aeruginosa* by its hemophore (HasAp) bound to synthetic metal complexes, Angew. Chem. 126 (11) (2014) 2906–2910.
[41] V. Bogoeva, M. Siksjø, K.G. Sæterbø, T.B. Melø, A. Bjørkøy, M. Lindgren, et al., Ruthenium porphyrin-induced photodamage in bladder cancer cells, Photodiagn. Photodyn. Ther. 14 (2016) 9–17.
[42] M.B. Winter, E.J. McLaurin, S.Y. Reece, C. Olea Jr., D.G. Nocera, M.A. Marletta, Ru-porphyrin protein scaffolds for sensing O2, J. Am. Chem. Soc. 132 (16) (2010) 5582–5583.
[43] V. Artero, M. Chavarot-Kerlidou, M. Fontecave, Splitting water with cobalt, Angew. Chem. Int. Ed. 50 (32) (2011) 7238–7266.
[44] M. Kathiresan, B. Ambrose, N. Angulakshmi, D.E. Mathew, D. Sujatha, A. M. Stephan, Viologens: a versatile organic molecule for energy storage applications, J. Mater. Chem. A 9 (48) (2021) 27215–27233.
[45] J. Ding, C. Zheng, L. Wang, C. Lu, B. Zhang, Y. Chen, et al., Viologen-inspired functional materials: synthetic strategies and applications, J. Mater. Chem. A 7 (41) (2019) 23337–23360.
[46] A.Y. Alontaga, J.C. Rodriguez, E. Schönbrunn, A. Becker, T. Funke, E.T. Yukl, et al., Structural characterization of the Hemophore HasAp from *Pseudomonas aeruginosa*: NMR spectroscopy reveals protein− protein interactions between Holo-HasAp and hemoglobin, Biochemistry 48 (1) (2009) 96–109.
[47] E.A. Brucker, J.S. Olson, G.N. Phillips, Y. Dou, M. Ikeda-Saito, High resolution crystal structures of the deoxy, oxy, and aquomet forms of cobalt myoglobin, J. Biol. Chem. 271 (41) (1996) 25419–25422.
[48] N.J. Greenfield, Using circular dichroism spectra to estimate protein secondary structure, Nat. Protoc. 1 (6) (2006) 2876–2890.
[49] Z. Valicsek, O. Horváth, Application of the electronic spectra of porphyrins for analytical purposes: the effects of metal ions and structural distortions, Microchem. J. 107 (2013) 47–62.
[50] H. Anni, J.M. Vanderkooi, L. Mayne, Structure of zinc-substituted cytochrome c: nuclear magnetic resonance and optical spectroscopic studies, Biochemistry 34 (17) (1995) 5744–5753.
[51] L.J. Perkins, B.R. Weaver, A.R. Buller, J.N. Burstyn, De novo biosynthesis of a nonnatural cobalt porphyrin cofactor in *E. coli* and incorporation into hemoproteins, Proc. Natl. Acad. Sci. 118 (16) (2021) e2017625118.
[52] M.Z. Hoffman, D. Prasad, G. Jones, V. Malba, Formation of photoactive charge-transfer complexes between methyl viologen and sacrifical electron donors. EDTA and triethanolamine, J. Am. Chem. Soc. 105 (20) (1983) 6360–6362.
[53] J.P. Kuczynski, B.H. Milosavljevic, A.G. Lappin, J.K. Thomas, Ion-pair complexes of methyl viologen and anionic solutes, Chem. Phys. Lett. 104 (2) (1984) 149–152.
[54] E.H. Edwards, J. Jelušić, S. Chakraborty, K.L. Bren, Photochemical hydrogen evolution from cobalt microperoxidase-11, J. Inorg. Biochem. 217 (2021) 111384.
[55] R. Bauer, A new mechanism for electron transfer between methyl viologen radicals and water, J. Mol. Catal. 72 (1) (1992) 67–74.